Optical Trapping in a Dark Focus

B. Melo,[1,*] I. Brandão,[1,†] B. Pinheiro da Silva,[2,‡] R.B. Rodrigues,[2,§] A.Z. Khoury,[2,¶] and T. Guerreiro[1,‖]

[1] *Departamento de Física, Pontifícia Universidade Católica do Rio de Janeiro, Rio de Janeiro, Rio de Janeiro 22451-900, Brazil*

[2] *Instituto de Física, Universidade Federal Fluminense, Niterói, Rio de Janeiro 24210-346, Brazil*

(Received 30 June 2020; revised 31 July 2020; accepted 26 August 2020; published 30 September 2020)

The superposition of a Gaussian mode and a Laguerre-Gauss mode with $\ell = 0, p \neq 0$ generates the so-called bottle beam: a dark focus surrounded by a bright region. In this paper, we theoretically explore the use of bottle beams as an optical trap for dielectric spheres with a refractive index smaller than that of their surrounding medium. The forces acting on a small particle are derived within the dipole approximation and used to simulate the Brownian motion of the particle in the trap. The intermediate regime of particle size is studied numerically and it is found that stable trapping of larger dielectric particles is also possible. Based on the results of the intermediate-regime analysis, an experiment aimed at trapping living organisms in the dark focus of a bottle beam is proposed.

DOI: 10.1103/PhysRevApplied.14.034069

I. INTRODUCTION

Tightly focused laser beams can be used to exert forces upon dielectric particles. If the refractive index of the particle is *larger* than that of its surroundings, the laser pulls it to regions of higher intensity of light. This technique, introduced by Ashkin in 1986 [1] and known today as optical tweezing, allows one to hold and manipulate very tiny objects and finds applications in a large number of fields ranging from biology [2–5] to fundamental physics [6–10]. In standard optical tweezers, Gaussian beams are used to create the trapping focus. To a good approximation, the trap can be described as a three-dimensional quadratic potential.

Notably, it has also been pointed out by Ashkin that air droplets immersed in water are pushed away from the Gaussian focus [11]. This is a consequence of the fact that when the refractive index of the particle is *smaller* than that of its surroundings, the particle is repelled from the region of high intensity. One can then envision an *inverted* optical trap, in which an engineered beam of light has a high-intensity boundary and a dark focus. A particle with the appropriate refractive index will be trapped within the dark focus by the absence of light [12]. We refer to this type of beam, which has first been proposed as a tool to trap atoms [13–16], as a *bottle beam*. A bottle beam such as the one proposed in [17] is one example in a myriad of engineered optical traps aimed at different purposes such as Bessel beams [18], frozen waves [19], circular Airy beams [20–22], radially polarized beams [23,24], and many others [25–30].

Several techniques can be employed to create bottle beams, such as the generation of Bessel beams using axicons [31–33], the interference of Gaussian beams of different waists [34], and the superposition of different modes [35–37] created using spatial light modulators (SLMs). Here, we focus on the bottle beam created by the superposition of a Gaussian beam and a Laguerre-Gauss beam with $\ell = 0, p \neq 0$ and a relative phase of π presented in [17] and study the optical forces it exerts upon low-refractive-index particles.

The superposition of a Gaussian mode and a Laguerre-Gaussian beam with $\ell = 0, p \neq 0$ is an interesting choice for a number of reasons. First, as we show, it yields a simple mathematical description from which the trapping potential can be readily obtained. Moreover, description of the trap in terms of its width, height, and shape is simple and clearly defined. Furthermore, such superposition is promptly obtained by the use of a SLM, a well-established technique for engineering structured light beams available in the laboratory [38–41].

Because optical trapping can be applied to particles in a wide size range [42,43], we analyze both the cases of small Rayleigh particles and of larger micron-sized particles. In the former, the optical forces and potential are derived from the dipole approximation and thoroughly analyzed under different assumptions, which are verified

[*] bruno.b.fernando.f@gmail.com
[†] igorbrandao@aluno.puc-rio.br
[‡] braianps@gmail.com
[§] rafaelbellasrodrigues@gmail.com
[¶] azkhoury@id.uff.br
[‖] barbosa@puc-rio.br

by simulating the motion of the trapped particle in a viscous medium. In the latter, generalized Lorenz-Mie theory is employed to calculate the forces caused by the beam, with the aid of the tools introduced in Ref. [44]. Constraints on the numerical aperture, particle size, and relative refractive index are found.

An understanding of particle dynamics under the influence of a bottle beam can lead to striking applications. Notably, the bottle is an interesting tool for trapping experiments requiring little or no light scattering upon the trapped object. This is of particular interest in biology, where trapping a living cell or organelles within the cell without the constant influence of laser light might be crucial in revealing the mechanical properties of the organism without excessive heating and laser interference [45–47]. We thus propose a set of experimental parameters that could be used to trap living organisms in the dark focus of a bottle beam.

II. THE DIPOLE APPROXIMATION

We begin by investigating the optical forces acting on a Rayleigh particle with a refractive index lower than its surrounding medium under the dipole approximation. This is valid when the radius of the trapped particle is much smaller than the wavelength of the trapping laser ($R \lesssim \lambda/10$) [48].

A. The optical bottle beam

To generate a dark focus surrounded by a bright region, we superpose a Laguerre-Gauss beam with $\ell = p = 0$—a Gaussian beam—and a Laguerre-Gauss beam with $\ell = 0, p \neq 0$ and a relative phase of π. The electric field magnitude of a Laguerre-Gauss (LG) beam is

$$
\begin{aligned}
E^{\mathrm{LG}}_{\ell,p}(\rho,\phi,z) = &\sqrt{\frac{4P_0}{c\epsilon\pi\omega(z)^2}}\sqrt{\frac{p!}{(|\ell|+p)!}} \\
&\times\left(\frac{\sqrt{2}\rho}{\omega(z)}\right)^{|\ell|} L_p^{|\ell|}\left(\frac{2\rho^2}{\omega(z)^2}\right)\exp\left[-\frac{\rho^2}{\omega(z)^2}\right] \\
&\times\exp\left[ik_m z + ik_m\frac{\rho^2}{2R(z)} - i\zeta(z) + i\ell\phi\right],
\end{aligned}
\tag{1}
$$

where c is the speed of light, ϵ is the permittivity of the medium, P_0 is the laser power, k_m is the wave number in the medium and $\omega(z)$, $R(z)$, $\zeta(z)$ and $L_p^{|\ell|}$ are the beam width, the wave-front radius, the Gouy phase, and the associated Laguerre polynomial. These quantities are, respectively, given by

$$\omega(z) = \omega_0\sqrt{1+\frac{z^2}{z_R^2}}, \tag{2}$$

$$R(z) = z\left(1+\frac{z_R^2}{z^2}\right), \tag{3}$$

$$\zeta(z) = (2p+|\ell|+1)\arctan\frac{z}{z_R}, \tag{4}$$

$$L_p^{|\ell|}(x) = \sum_{i=0}^{p}\frac{1}{i!}\binom{p+|\ell|}{p-i}(-x)^i, \tag{5}$$

where the Rayleigh range (z_R) and the beam waist (ω_0) are defined as

$$\omega_0 = \frac{\lambda_0}{\pi\mathrm{NA}}, \quad z_R = \frac{n_m\lambda_0}{\pi\mathrm{NA}^2}, \tag{6}$$

in which λ_0 is the wavelength in vacuum, n_m is the refractive index of the medium, and NA is the numerical aperture. Throughout this paper, we consider linearly polarized electric fields only.

The intensity of the bottle beam reads

$$
\begin{aligned}
I_p(\rho,z) = &I_0\frac{\omega_0^2}{\omega(z)^2}\exp\left[-\frac{2\rho^2}{\omega(z)^2}\right] \\
&\times\left[1 - 2\cos\left(2p\arctan\frac{z}{z_R}\right)L_p^0\left(\frac{2\rho^2}{\omega(z)^2}\right)\right. \\
&\left.+L_p^0\left(\frac{2\rho^2}{\omega(z)^2}\right)^2\right],
\end{aligned}
\tag{7}
$$

where $I_0 = 2P_0/\pi\omega_0^2$ is the intensity at the origin of the Gaussian beam. Figures 1(a) and 1(b) show the intensity as a function of the transverse coordinate x and the longitudinal coordinate z. The potential landscape in the x-z plane is shown in Fig. 1(c) for the case $p = 1$ and in Fig. 1(d) for the case $p = 2$. A dielectric particle with the appropriate refractive index placed at the origin would be trapped in the dark focus, since it would be repelled in all directions by the surrounding regions of higher electromagnetic intensity.

B. Dimensions of the bottle

We can define the width W (height H) of the bottle as the distance between the two intensity maxima surrounding the dark region along the x axis (z axis). These values can be found by solving

$$dI_p(x,0,0)/dx|_{x=W/2} = 0, \tag{8}$$

$$dI_p(z,0,0)/dz|_{z=H/2} = 0. \tag{9}$$

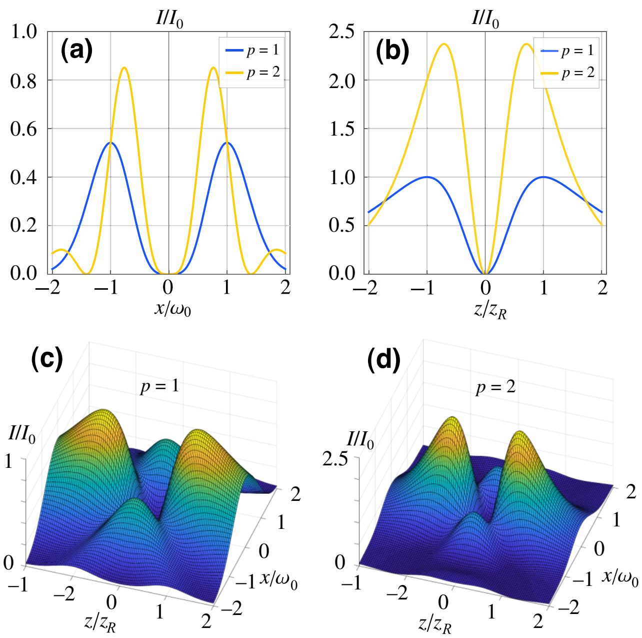

FIG. 1. The intensity in the (a) radial and (b) axial directions for bottle beams with $p = 1$ and $p = 2$. The intensity landscape in the x-z plane for bottle beams with (c) $p = 1$ and (d) $p = 2$. Due to the normalization of x, z, and I, these plots depend only on p and are independent of the remaining beam parameters.

The above equations admit analytical solutions for small p, yielding $W = 2\omega_0, H = 2z_R$ for $p = 1$ and $W = 2\sqrt{2-\sqrt{2}}\omega_0, H = \sqrt{2}z_R$ for $p = 2$.

To gain insight into H and W, it is useful to make the change of variables $\rho/\omega_0 \to \rho', z/z_R \to z'$ in the intensity given in Eq. (7). The function $I_p(\rho', z')$ has no explicit dependence on any of the beam's parameters other than p and I_0, with its associated rescaled width W' and height H'. The prefactor I_0 does not alter the distance between maxima along the x' and z' axes, meaning that $W' = W'(p)$ and $H' = H'(p)$ depend only on p. Going back to the original variables, we find that $W = \omega_0 W'(p)$ and $H = z_R H'(p)$. From Eq. (6), we observe that the width of the bottle scales with NA^{-1} and the height scales with NA^{-2}. Hence an increase in NA causes the bottle to become smaller overall and compressed along the z direction.

C. Radiation forces

When a Rayleigh particle is placed in an electromagnetic field, there are three forces that act on it [49]. The first, called the spin-curl force, is a result of polarization gradients [50] and can be disregarded in the case of uniform linear polarization in which we are interested. The second is called the scattering force and is proportional to the Poynting vector. Near the origin, the scattering force points in the direction of propagation of the beam. Finally, the gradient force is proportional to the gradient of the potential energy of the particle under the influence of the electromagnetic field. From the intensity given by Eq. (7), the scattering force $\vec{F}_p^{(\mathrm{scat})}(\vec{r})$, the gradient force $\vec{F}_p^{(\mathrm{grad})}(\vec{r})$, and the optical potential $V_p(\vec{r})$ acting on a trapped particle with radius R and refractive index n_p can be readily calculated using [48]

$$\vec{F}_p^{(\mathrm{scat})}(\vec{r}) = \hat{z}\,\frac{128\pi^5 R^6}{3c\lambda_0^4}\left(\frac{m^2-1}{m^2+2}\right)^2 n_m^5 I_p(\vec{r}), \qquad (10)$$

$$\vec{F}_p^{(\mathrm{grad})}(\vec{r}) = \frac{2\pi n_m R^3}{c}\left(\frac{m^2-1}{m^2+2}\right)\nabla I_p(\vec{r}), \qquad (11)$$

$$V_p(\vec{r}) = -\frac{2\pi n_m R^3}{c}\left(\frac{m^2-1}{m^2+2}\right) I_p(\vec{r}), \qquad (12)$$

where $m = n_p/n_m$ is the particle-medium refractive-index ratio. We are interested in situations in which the parameter m is smaller than 1, in such a way that the particle is repelled by light.

The forces acting on a spherical water droplet ($n_p = 1.33$) with 70-nm radius trapped in oil ($n_m = 1.46$) by a bottle beam ($\lambda = 780$ nm, $P_0 = 200$ mW for each beam in the superposition) focused by an objective lens (NA = 0.5) are displayed in Fig. 2. As expected, the gradient forces point to the origin. Note that the scattering force, which points along the propagation direction, is null at the equilibrium position. This is in strong contrast to standard Gaussian traps and presents an advantage, since the imbalance between scattering and gradient forces often poses challenges to optical trapping [51].

Another interesting feature of the bottle-beam trap is the flat bottom of the intensity well in the $z = 0$ plane, seen in Fig. 1(a), and the approximate null derivative of the force along the radial direction at the origin. This can be understood by looking at the potential near the origin ($\rho \ll \omega_0$, $z \ll z_R$). It can be approximated to fourth order as

$$\frac{V_p(\rho,z)}{V_0} \approx \underbrace{\frac{4p^2}{\omega_0^4}\rho^4}_{T_{\rho^4}} - \underbrace{\frac{8p^2(p+1)}{\omega_0^2 z_R^2}\rho^2 z^2}_{T_{\rho^2 z^2}} + \underbrace{\frac{4p^2}{z_R^2}z^2}_{T_{z^2}}, \qquad (13)$$

where $V_0 = [2\pi n_m R^3(m^2-1)/c(m^2+2)]I_0$ and the term of order $\mathcal{O}[(z/z_R)^4]$ has been neglected, since $(z/z_R)^4 \ll (z/z_R)^2$ for $z \ll z_R$. At the plane $z = 0$, the potential scales with ρ^4. Therefore, the force scales with ρ^3 and has vanishing first and second derivatives. For $z \neq 0$, Eq. (13) has a crossed term $\rho^2 z^2$ that couples motion along the axial and radial directions. Because the scattering force is proportional to the intensity, it also has null derivatives at the equilibrium position and hence it vanishes for a particle placed at and near the origin.

Finally, the potential in the x-z plane is displayed in Figs. 2(c) and 2(d) for the cases of $p = 1$ and $p = 2$. As can

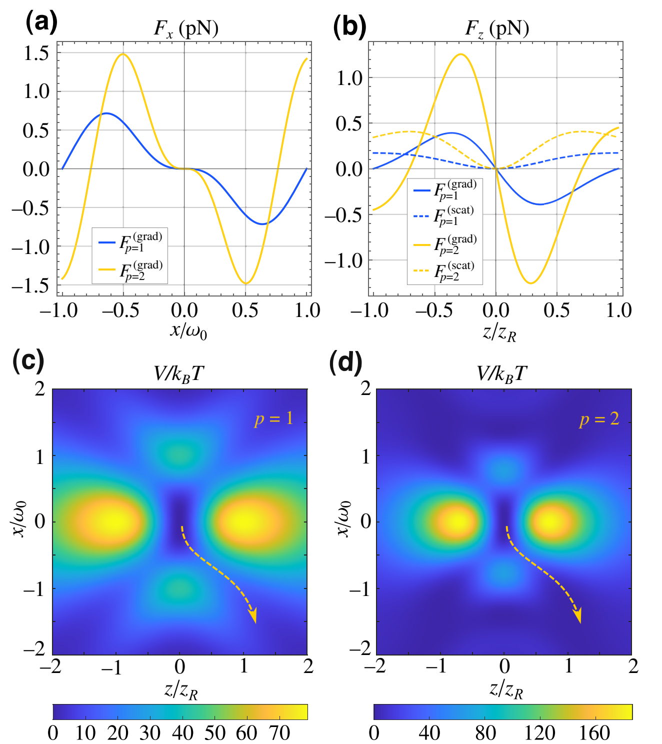

FIG. 2. The forces acting on a trapped sphere in the (a) x direction and (b) z direction for $p = 1$ and $p = 2$. The solid lines are gradient forces, while the dashed lines are scattering forces. The potential landscape in the x-z plane for a sphere trapped by a bottle beam with (c) $p = 1$ and (d) $p = 2$. The parameters used for these plots are NA $= 0.5$, $R = 70$ nm, $\lambda_0 = 780$ nm, $n_m = 1.46$, $n_p = 1.33$, $P_0 = 200$ mW, and $T = 300$ K.

be seen, a trapped particle does not need to go through the high-intensity peaks along the x or z axis in order to escape the trap. Smaller potential barriers have to be climbed if the particle undergoes paths such as the yellow dashed ones. We call the lowest potential energy needed for the particle to leave the trap $V_{\min}$. Because the potential scales with V_0, we have $V_{\min} \propto V_0$.

D. Decoupling approximation

The axial and radial movements can be decoupled if the coupling term in Eq. (13) is much smaller than the remaining terms. The conditions under which this assumption holds true can be found by estimating the magnitude of the displacements of the particle under the influence of the trap. Neglecting the cross term and considering thermal equilibrium, we may write

$$\langle \rho^4 \rangle = \frac{1}{Z_0} \int d^3\vec{r} \rho^4 \exp\left[-\frac{4V_0 p^2}{k_B T} \left(\frac{\rho^4}{\omega_0^4} + \frac{z^2}{z_R^2} \right) \right], \quad (14)$$

$$\langle z^2 \rangle = \frac{1}{Z_0} \int d^3\vec{r} z^2 \exp\left[-\frac{4V_0 p^2}{k_B T} \left(\frac{\rho^4}{\omega_0^4} + \frac{z^2}{z_R^2} \right) \right], \quad (15)$$

where k_B is the Boltzmann constant, T is the temperature, and Z_0 is given by

$$Z_0 = \int d^3\vec{r} \exp\left[-\frac{4V_0 p^2}{k_B T} \left(\frac{\rho^4}{\omega_0^4} + \frac{z^2}{z_R^2} \right) \right]. \quad (16)$$

From Eqs. (14)–(16), we find that

$$\sqrt[4]{\langle \rho^4 \rangle} = \sqrt[4]{\frac{\omega_0^4 k_B T}{8p^2 V_0}}, \quad (17)$$

$$\sqrt{\langle z^2 \rangle} = \sqrt{\frac{z_R^2 k_B T}{8p^2 V_0}}. \quad (18)$$

Although Eqs. (17) and (18) are derived by neglecting the cross term, they can be used to estimate the magnitude of the three different terms in Eq. (13). Through simple scaling, we are led to

$$\frac{T_{\rho^2 z^2}}{T_{\rho^4}} \sim \frac{T_{\rho^2 z^2}}{T_{z^2}} \sim \frac{1+p}{\sqrt{2p}} \left(\frac{V_0}{k_B T} \right)^{-1/2}. \quad (19)$$

Because $V_{\min}/k_B T \gg 1$ is required for the particle to be confined in the presence of a thermal bath [48] and $V_{\min} \propto V_0$, fulfillment of the decoupling condition is associated with increased trap stability.

In the decoupling regime, the optical potential becomes

$$V_p(\rho, z) \approx \frac{k_\rho^{(3)}}{4} \rho^4 + \frac{k_z}{2} z^2, \quad (20)$$

with the constants $k_\rho^{(3)}$ and k_z given by

$$k_\rho^{(3)} = \frac{64 n_m P_0 R^3}{c} \left(\frac{\pi \mathrm{NA}}{\lambda_0} \right)^6 \left(\frac{1-m^2}{2+m^2} \right) p^2, \quad (21)$$

$$k_z = \frac{32 P_0 R^3 \lambda_0^2}{\pi^2 n_m c} \left(\frac{\pi \mathrm{NA}}{\lambda_0} \right)^6 \left(\frac{1-m^2}{2+m^2} \right) p^2. \quad (22)$$

E. Trapped particle dynamics

To further evaluate the validity of the above estimates and approximations, it is useful to simulate the dynamics of a particle trapped by the potential of a bottle beam in its exact form, calculated from Eqs. (7) and (12). The equation of motion for a spherical particle under this condition is

$$M\ddot{\vec{r}}(t) = -\gamma \dot{\vec{r}}(t) - \nabla V(\vec{r}(t)) + \sqrt{2\gamma k_B T} \vec{W}(t), \quad (23)$$

where η is the viscosity of the medium, $\gamma = 6\pi\eta R$ is the drag coefficient, and M is the mass of the particle. The environmental fluctuations are modeled using a

Gaussian, white, and isotropic stochastic process $\vec{W}(t) = (W_x(t), W_y(t), W_z(t))$, with zero mean and no correlations among different directions. We have that

$$\langle W_i(t)W_i(t')\rangle = \delta(t-t'), \tag{24}$$

where $\delta(t-t')$ is the Dirac delta in the time domain.

For a sufficiently small particle, the inertial term $M\ddot{\vec{r}}$ is negligible in comparison to the viscous term $\gamma\dot{\vec{r}}$. In this so-called *overdamped* regime, we can numerically integrate Eq. (23) using

$$\vec{r}(t+\Delta t) = \vec{r}(t) - \frac{\nabla V[\vec{r}(t)]}{\gamma}\Delta t + \sqrt{\frac{2k_B T\Delta t}{\gamma}}\vec{W}(t), \tag{25}$$

where $\Delta t = \tau/n$ is the time interval between iterations, τ is the total time of simulation, and n is the total number of iterations.

Numerical integration of the motion of a water droplet ($n_p = 1.33$, $R = 70$nm) trapped in oil ($n_m = 1.46$) by a bottle beam ($p = 1$, $\lambda = 780$ nm) focused using an objective lens (NA $= 0.5$) is performed for different trapping powers. Note that the total trapping power is twice as large as the power P_0 of each beam (for details, see Appendix A).

The motion is simulated for a period of 10 s, using time steps of 0.5 μs. This results in 20×10^6 position values for each trapping power. The values of $\sqrt[4]{\langle x^4\rangle}$ and $\sqrt{\langle z^2\rangle}$ obtained from this simulation of the exact potential and the curves predicted using the approximated potential in Eq. (20) together with Eqs. (14) and (15) are displayed in Fig. 3. The largest values of $\sqrt[4]{\langle x^4\rangle}/\omega_0$ and $\sqrt{\langle z^2\rangle}/z_R$ obtained are approximately 0.27 and 0.067, respectively. This justifies the fourth-order approximation leading to Eq. (13) for the entire simulated range of trapping powers.

Moreover, we can see from Fig. 3 that agreement between the simulated dynamics of the exact potential and the approximate potential of Eq. (20) increases with P_0. For $P_0 > 1$ W, the exact and approximate values differ by less than 3% and hence Eq. (20) can be considered a good approximation of the potential. This behavior is consistent with the previous estimate that the ratios $T_{\rho^2 z^2}/T_{\rho^4}$ and $T_{\rho^2 z^2}/T_{z^2}$ scale with $V_0^{-1/2}$ and, hence, the larger the trapping power, the smaller the cross term in comparison to the remaining relevant terms.

This can be further verified in Fig. 4, where we plot the ratios

$$r_1 = \frac{\langle T_{\rho^2 z^2}\rangle}{\langle T_{\rho^4}\rangle}, \quad r_2 = \frac{\langle T_{\rho^2 z^2}\rangle}{\langle T_{z^2}\rangle} \tag{26}$$

obtained from the simulations. The decreasing behavior of r_1 and r_2 with respect to P_0 confirms that increasing the trapping power is an effective way of decoupling the radial and axial directions.

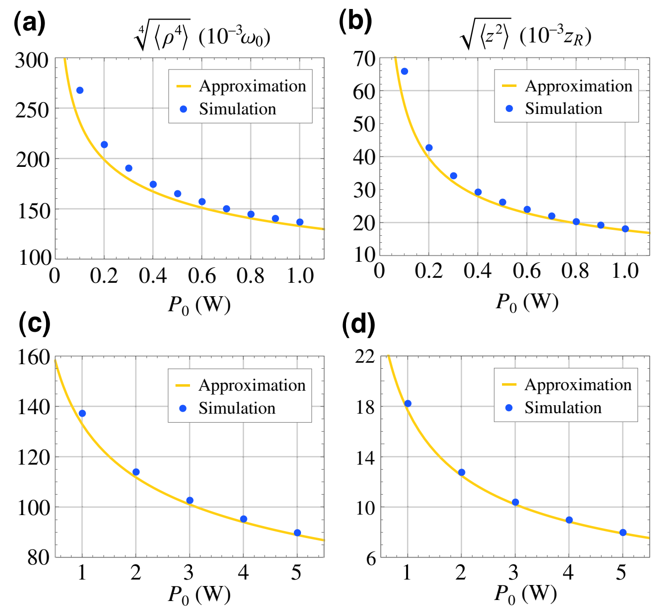

FIG. 3. A comparison between the values of (a),(c) $\sqrt[4]{\langle\rho^4\rangle}$ and of (b),(d) $\sqrt{\langle z^2\rangle}$ obtained from the approximated potential in Eq. (20) and from simulation of the motion of the particle subject to the exact potential in Eq. (12) for different laser powers. The motion is simulated during a period of 10 s, with time steps of 0.5 μs, using NA $= 0.5$, $R = 70$ nm, $\lambda_0 = 780$ nm, $n_m = 1.46$, $n_p = 1.33$, $T = 295$ K, and $p = 1$.

Another consequence of the interplay between a radial quartic and a longitudinal quadratic potential is that the elongation of the trap can be adjusted by tuning the laser power. This is illustrated in Fig. 5, in which the positions of the trapped particle obtained from the numerical simulation are displayed in a scatter plot, for $P_0 = 100$ mW and $P_0 = 5$ W. As can be seen, the trap is appreciably

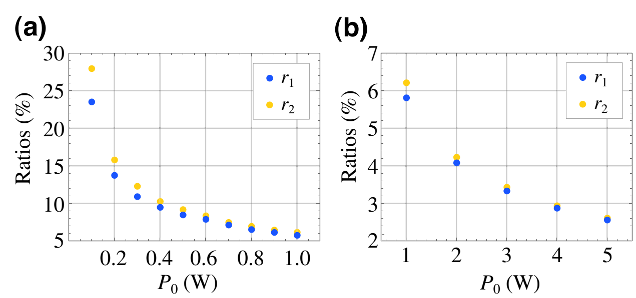

FIG. 4. The ratios $r_1 = \langle T_{\rho^2 z^2}\rangle/\langle T_{\rho^4}\rangle$ and $r_2 = \langle T_{\rho^2 z^2}\rangle/\langle T_{z^2}\rangle$ obtained by simulating the motion of a particle subject to the exact potential in Eq. (12) for different laser powers. The motion is simulated during a period of 10 s, with time steps of 0.5 μs, using NA=0.5, $R = 70$ nm, $\lambda_0 = 780$ nm, $n_m = 1.46$, $n_p = 1.33$, and $T = 295$ K.

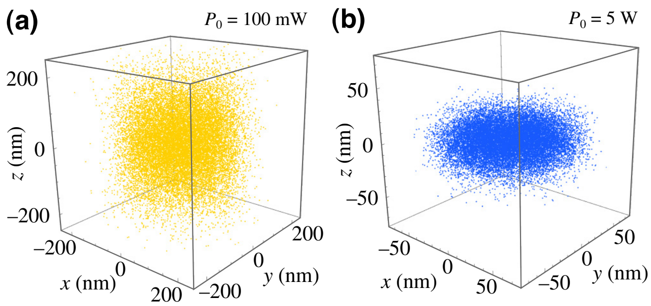

FIG. 5. The positions of the particle obtained by simulating the motion of a particle trapped by the exact potential in Eq. (12) for (a) $P_0 = 100$ mW and (b) $P_0 = 5$ W. The motion is simulated during a period of 10 s, with time steps of 0.5 μs, using $\mathrm{NA} = 0.5$, $R = 70$ nm, $\lambda_0 = 780$ nm, $n_m = 1.46$, $n_p = 1.33$, $T = 295$ K, and $p = 1$. To allow better visualization, the 20×10^6 positions generated by the simulation are divided in 1000 sets and only the first value of each set is displayed in the figure.

compressed along the z axis in the latter case but not in the former. This feature is not present in regular Gaussian tweezers: since the potential is quadratic along the three axis, the expected values of the displacement along all axes scale equally with $\sqrt{P}$.

We note that this compression is different from that caused by an increase in numerical aperture, mentioned previously. In that case, we have a compression of the overall shape of the intensity landscape along the z axis, which happens in the case of a Gaussian beam due to the scaling of ω_0 with NA^{-1} and of z_R with NA^{-2}. In contrast, an increase in the trapping power of a bottle beam compresses the region visited by the particle over time.

In summary, we conclude that in the dipole regime given in Eq. (13) is a good approximation for the optical potential generated by a bottle beam for a wide range of trapping powers, as it only relies on $\rho^4/\omega_0^4 \ll 1$ and $z^4/z_R^4 \ll 1$. On the other hand, decoupling of the radial and axial motions only occurs for high trapping powers that make the cross term in Eq. (13) negligible. This allows approximation of the potential by Eq. (20). Furthermore, increasing the trapping power causes squashing along the axial direction of the accessible region for a trapped particle.

F. Decoupling by addition of an extra mode

High trapping powers are only necessary if one wishes to decouple the radial and axial dependencies of the trapping potential but when considering power-sensitive samples, such as biological ones, this is not viable. An alternative, which is valid independent of the trapping power, is to add an extra Laguerre-Gauss mode with $\ell_2 = 0$ and $p_2 \neq 0$ to the superposition. Consider the intensity $I(\rho, z)$ of the following superposition:

$$E(\rho, z) = E_{0,0}^{\mathrm{LG}}(\rho, z) + \alpha_1 E_{0,1}^{\mathrm{LG}}(\rho, z) + \alpha_2 E_{0,p_2}^{\mathrm{LG}}(\rho, z), \quad (27)$$

where $\alpha_{j=1,2}$ are complex amplitudes. The condition to have a bottle beam is that $I(\rho, z)$ vanishes at the focus. The light intensity at the beam focus is proportional to

$$I(\mathbf{0}) = \mathcal{N}^2 \left|1 + \alpha_1 + \alpha_2\right|^2, \quad (28)$$

where $\mathcal{N} = \sqrt{4P_0/c\epsilon\pi\omega_0^2}$.

With the appropriate approximations (for details, see Appendix B) and the bottle-beam condition in Eq. (28), we obtain the approximate intensity $I(\rho, z)$:

$$\mathcal{N}^2 \left[4|B|^2 \left(\frac{z^2}{z_R^2} + \frac{\rho^4}{w_0^4} \right) - 8 \left[|B|^2 + \mathrm{Re}\left(AB^* \right) \right] \frac{z^2 \rho^2}{z_R^2 w_0^2} \right], \quad (29)$$

where $A = \alpha_1 + \alpha_2 p_2^2$ and $B = \alpha_1 + \alpha_2 p_2$. Decoupling of the radial and longitudinal motions can then be achieved by choosing α_1 and α_2 such that

$$|B|^2 + \mathrm{Re}\left(AB^* \right) = 0 \quad (B \neq 0). \quad (30)$$

As an example, let us choose $p_2 = 2$. A decoupled bottle beam can be obtained by the superposition coefficients

$$\alpha_1 = -3/2, \quad (31)$$

$$\alpha_2 = 1/2. \quad (32)$$

Using Eq. (12), we can find the decoupled potential near the origin ($\rho \ll \omega_0$, $z \ll z_R$). This is given to fourth order by

$$V(\rho, z) \approx V_0 \left(\frac{z^2}{z_R^2} + \frac{\rho^4}{w_0^4} \right), \quad (33)$$

which has the same form as Eq. (20). Moreover, this solution yields the maximum trap stiffness of the three-mode configuration, as demonstrated in Appendix B.

G. Calibration of the optical trap

In laboratory conditions, quantitative measurements using optical tweezers rely on knowledge of the trap's parameters. In the case of a bottle trap defined by the potential in Eq. (20), the relevant parameters are k_z and $k_\rho^{(3)}$. To operate the tweezer properly, these must be found by measuring the position of the particle during a finite interval of time. This yields a time series $\vec{r}_m(t) = \vec{\beta} \cdot \vec{r}(t)$, where $\vec{\beta} = (\beta_x, \beta_y, \beta_z)$ are conversion factors between position displacements and the measured quantity, such as the voltage in a position-sensitive detector. For simplicity, we assume $\beta_x = \beta_y = \beta_\rho$.

For a bottle-beam trap, the position of the particle can be measured using a high-speed camera [52] or, alternatively, by applying a purely Gaussian beam at a different wavelength with respect to the bottle beam. The second beam can be focused onto the trapped particle by the same objective lens used for the bottle and collected by a second objective lens after separation from the trapping beam by a dichroic mirror. The collected Gaussian light can then be directed onto a quadrant photodetector, where the usual forward-scattering measurement is performed [53]. The Gaussian power should be kept significantly weaker than the bottle power to avoid disturbances due to the presence of this auxiliary Gaussian trap.

In the decoupled regime, movement along the z axis is independent of movement along the x and y axes and the equations of motion can be separated from Eq. (23), yielding

$$-\gamma \dot{z}(t) - k_z z(t) + \sqrt{2\gamma k_B T} W_z(t) = 0, \tag{34}$$

where, once again, we assume that the inertial term is negligible. The constants k_z and β_z can be found using the standard procedure of analyzing the autocorrelation function [54] or the power spectral density [55,56] of the measured axial displacements $z_m(t) = \beta_z z(t)$.

To find the remaining relevant constants, we need two independent equations. Using Eqs. (14) and (21), we may write

$$\frac{k_\rho^{(3)}\langle\rho^4\rangle}{4} = \frac{k_B T}{2} \rightarrow \langle\rho^4\rangle = \frac{2k_B T}{k_\rho^{(3)}}, \tag{35}$$

leading to the relation

$$\langle\rho_m^4\rangle = \beta_\rho^4 \frac{2k_B T}{k_\rho^{(3)}}. \tag{36}$$

A second equation can be obtained from an active method of calibration consisting of moving the sample in which the particle is immersed with a known velocity $\vec{v}_{\text{drag}}$ [57,58]. This will cause a constant drag force $\gamma\vec{v}_{\text{drag}}$ on the particle and, taking $\vec{v}_{\text{drag}} = v_{\text{drag}}\hat{x}$ as the equation of motion along the x axis, becomes

$$\gamma v_{\text{drag}} - \gamma\dot{x}(t) - k_\rho^{(3)} x(t)\rho(t)^2 + W_x(t) = 0. \tag{37}$$

After a transient time, the particle reaches an equilibrium position displaced with respect to the trap's center, with $\langle\dot{x}(t)\rangle = 0$. Taking the time average of Eq. (37) leads to

$$\gamma v_{\text{drag}} - k_\rho^{(3)}\langle x(t)\rho(t)^2\rangle = 0, \tag{38}$$

which can then be used to obtain the relation

$$\langle x_m(t)\rho_m(t)^2\rangle = \beta_\rho^3 \frac{\gamma v_{\text{drag}}}{k_\rho^{(3)}}. \tag{39}$$

Equations (36) and (39) together with the standard autocorrelation procedure for the axial motion enables the measurement of the four parameters β_ρ, β_z, $k_\rho^{(3)}$, and k_z in the decoupled approximation.

III. INTERMEDIATE REGIME

In many applications, it is desirable to trap "large" micron-sized particles such as living cells [59,60]. This presents an intermediate regime, in which the size of the particle is comparable to the wavelength of the trapping beam ($R \approx \lambda$) and neither the dipole ($R \ll \lambda$) nor geometric optics ($R \gg \lambda$) approximations can be used to calculate the optical forces. Instead, the forces must be calculated using the so-called generalized Lorenz-Mie theory (GLMT), for which we provide a brief introduction following the treatment presented in Ref. [44].

A. Generalized Lorenz-Mie theory

Regardless of the size of the trapped particle, optical forces arise from the exchange of momentum with the photons from the trapping beam. Therefore, the total momentum transferred to the particle is equal to the change in momentum of the scattered electromagnetic field. It is then useful to separate the field into incoming $\vec{E}_{\text{in}}$ and outgoing $\vec{E}_{\text{out}}$ parts, which in turn can be expanded in terms of vector spherical wave functions (VSWFs) defined in a coordinate system centered at the center of the particle:

$$\vec{E}_{\text{in}} = \sum_{i=1}^{\infty}\sum_{j=-i}^{i} a_{ij}\vec{M}_{ij}^{(2)}(k\vec{r}) + b_{ij}\vec{N}_{ij}^{(2)}(k\vec{r}), \tag{40}$$

$$\vec{E}_{\text{out}} = \sum_{i=1}^{\infty}\sum_{j=-i}^{i} p_{ij}\vec{M}_{ij}^{(1)}(k\vec{r}) + q_{ij}\vec{N}_{ij}^{(1)}(k\vec{r}), \tag{41}$$

where $\vec{M}_{ij}^{(1)}, \vec{N}_{ij}^{(1)}, \vec{M}_{ij}^{(2)}$, and $\vec{N}_{ij}^{(2)}$ are the VSWFs, with superscript index "(1)" denoting outward-propagating transverse-electric and transverse-magnetic multipole fields and "(2)" denoting the corresponding inward-propagating multipole fields.

The coefficients a_{ij} and b_{ij} can be calculated for the incident beam and used to obtain the p_{ij} and q_{ij} coefficients for the scattered field by a simple matrix-vector multiplication between the so-called T matrix and a vector containing the coefficients of the incoming field. The T matrix depends only on the characteristics of the trapped particle, which we assume to be spherical. Once the coefficients are calculated, the force along the axial direction z

is given by

$$F_z = \frac{2n_{md}P}{cS}\sum_{i=1}^{\infty}\sum_{j=-1}^{i}\frac{j}{i(i+1)}\mathrm{Re}(a_{ij}^{*}b_{ij} - p_{ij}^{*}q_{ij}) - \frac{1}{i+1}\sqrt{\frac{i(i+2)(i-j+1)(i+j+1)}{(2i+1)(2i+3)}} \times \mathrm{Re}(a_{ij}a_{i+1,j}^{*} + b_{ij}b_{i+1,j}^{*} - p_{ij}p_{i+1,j}^{*} - q_{ij}q_{i+1,j}^{*}), \tag{42}$$

with

$$S = \sum_{i=1}^{\infty}\sum_{j=-i}^{i}(|a_{ij}|^2 + |b_{ij}|^2). \tag{43}$$

The forces acting along the x and y axes have more complicated formulas and can be more easily calculated by rotating the coordinate system. The effect of displacing the particle can be taken into account by appropriate translations of the trapping beam.

Due to the linearity of Eqs. (40) and (41), the expansion coefficients for a superposition of different beams can be found by adding the expansion coefficients for each beam and subsequently substituting in Eq. (42) to calculate the resultant force. To perform these computations for the case of a particle trapped by a bottle beam, we use the latest version of the toolbox developed in Ref. [44] .

B. Optical forces from a bottle beam

The optical forces generated by the superposition of a Gaussian beam and a Laguerre-Gauss beam with $\ell = 0, p \neq 0$ are obtained with the aid of Refs. [44,61]. For simplicity, we focus on the $p = 1$ case and a particle of refractive index $n_p = 1.33$ trapped by a 500-mW beam at $\lambda_0 = 780$ nm immersed in oil of refractive index $n_m = 1.46$.

Figure 6 shows the plots of $F_z(z)$ and $F_x(x)$ divided by the mass of the particle for four different NAs and four different particle radii. The force in the z direction is evaluated for $x = y = 0$, while $F_x(x)$ is evaluated at $y = 0, z = z_{\mathrm{eq}}$, where z_{eq} is the equilibrium coordinate along the z direction, i.e.,

$$\begin{cases} F_z(z_{\mathrm{eq}}) = 0, \\ dF_z(z)/dz|_{z=z_{\mathrm{eq}}} < 0. \end{cases} \tag{44}$$

When no equilibrium position exists, $F_x(x)$ is evaluated at $z = 0$.

Some general trends can be extracted from Fig. 6. First, we note that if the sphere is small ($R = \lambda_0/4$) and the numerical aperture is low ($\mathrm{NA} = 0.3, 0.5$), the force in

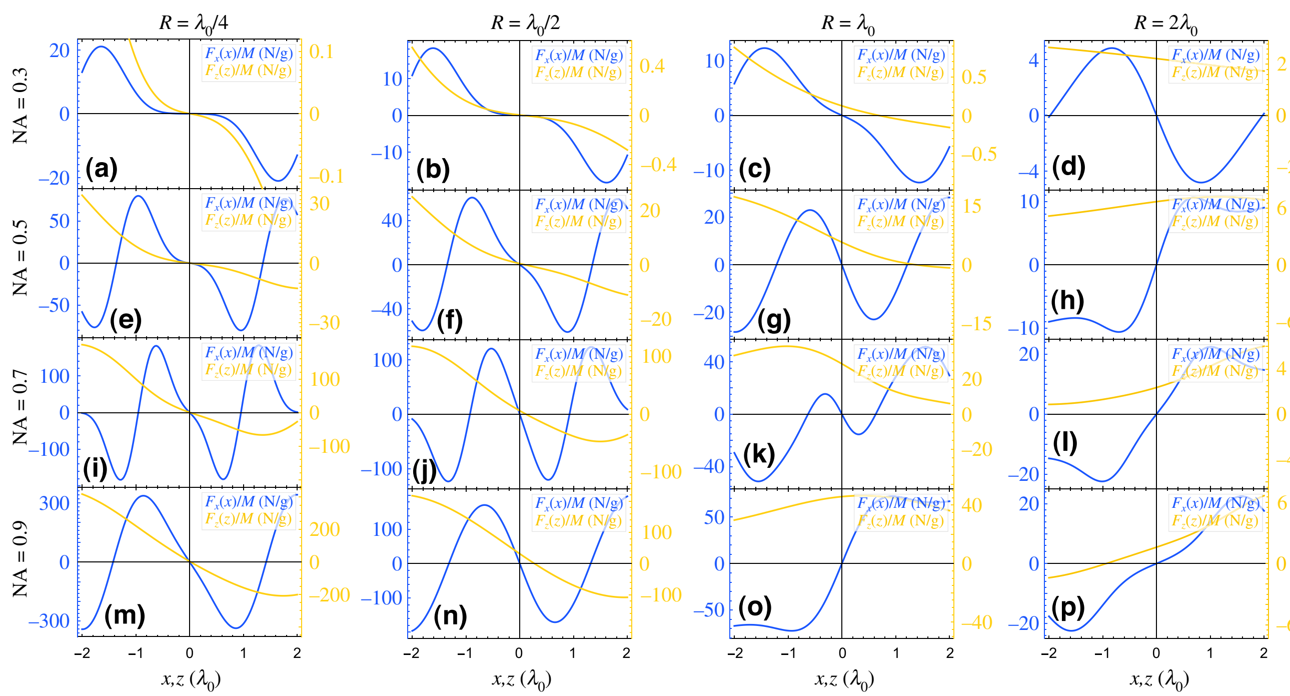

FIG. 6. The optical forces acting on a particle trapped by a bottle beam in the intermediate regime ($R \approx \lambda$). The force in the axial direction [$F_z(z)$] is calculated for $x = y = 0$, while the force in the radial direction [$F_x(x)$] is calculated for $y = 0$ and $z = z_{\mathrm{eq}}$. If no axial-equilibrium position is found, $F_x(x)$ is evaluated at $z = 0$. The radius of the particle is constant within each column, while the numerical aperture is constant within each line. The forces are normalized by the mass of the particle. The other parameters used in simulation are $n_p = 1.33$, $n_m = 1.46$, $\lambda_0 = 780$ nm, $P = 500$ mW, density of the particle $= 10^3$ kg/m^3, and $p = 1$.

the x direction resembles that calculated using the dipole approximation, i.e., it appears to scale with x^3 around the origin. As R or NA increases, this cubic dependence starts to vanish, giving way to a linear dependence.

We can also note that the size of the particle and the numerical aperture play important roles in the existence of an equilibrium position in the axial direction, with a large radius R and a large NA being detrimental to trap stability along the z axis. For NA $= 0.7$, for instance, there is an equilibrium position if $R = \lambda_0/4$ or $R = \lambda_0/2$ but not if R is larger. For a fixed $R = \lambda_0$, z_{eq} does not exist for NA > 0.5. This is rather different from what happens in the regular Gaussian trap, in which an increase in NA is associated with an increase in trap stability [48].

C. Limitations of trapping in a dark focus

The trends observed in Fig. 6 can be understood qualitatively by recalling that a bottle beam is a dark region surrounded by a finite bright-light boundary. If the particle is small enough, it will fit inside the dark region and will be repelled by the boundary. In contrast, if the particle is too big, it does not fit inside the bottle and the dark focus becomes irrelevant, with the beam effectively pushing the particle away.

This can be seen for in Figs. 6(e)–6(h): the dimensions of the bottle when NA $= 0.5$ are $W = 0.99\ \mu$m and $H = 2.9\ \mu$m. Therefore, a particle of diameter 0.5λ fits entirely inside the bottle and is free within the dark region, causing the force in the x direction to have a vanishing derivative near the origin. When $R = \lambda_0$, the particle no longer fits in the dark focus and the influence of light gives a linear scaling to $F_x(x)$ around the equilibrium position. When $R = 2\lambda_0$, the particle has an increased overlap with the light intensity and no longer encounters an equilibrium position.

Similarly, an increase in the numerical aperture causes the dark focus to shrink. When the bottle becomes too small to contain the particle, the situation in the third column of Fig. 6 is reached and the forces eventually turn into nonrestorative ones.

This qualitative reasoning is confirmed in Fig. 7, in which the equilibrium position z_{eq} and the derivative along the x direction near the equilibrium position are displayed as a function of the radius of the particle and the numerical aperture. Two main regions can be identified in each of the plots. The first of them is the region for which z_{eq} is not found in the range of inspected axial coordinates $-6\lambda_0 < z < 6\lambda_0$. In this region, the derivative along the x axis is not evaluated. The remaining areas are those in which an axial-equilibrium position exists.

Because we wish to trap the particle in the dark focus, we need to avoid equilibrium situations such as the ones described in Ref. [62] in the context of vortex beams, in which the scattering force is balanced by the repelling gradient force before the focus. To exclude trapping positions outside the bottle, the regions in which $z_{\mathrm{eq}} > H/2$ are displayed in dark gray and the regions in which $z_{\mathrm{eq}} < -H/2$ are displayed in light gray. In the latter case, the derivative of the radial force is found to be positive and hence nonrestorative, while in the former this derivative is found to be negative. The colored region, then, is the region for which stable trapping inside the bottle is possible.

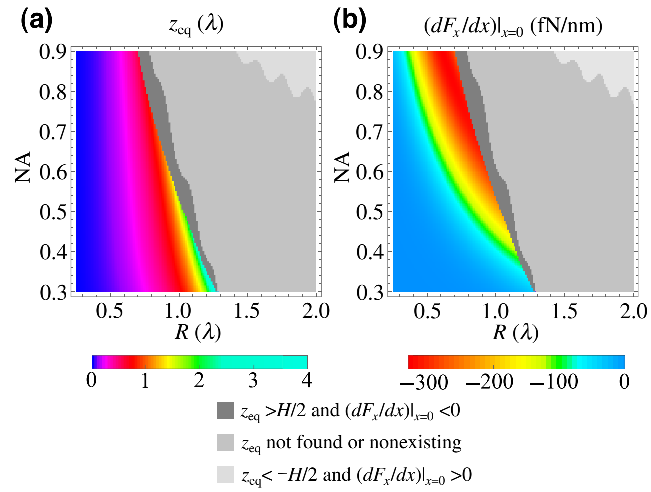

FIG. 7. Intermediate-regime simulations for different values of NA and R. (a) The axial-equilibrium coordinate and (b) the first derivative of the force in the radial direction: medium gray, no equilibrium position is found in the inspected range ($-6\lambda_0 < z < 6\lambda_0$); light (dark) gray, an equilibrium position is found outside the bottle, at $z_{\mathrm{eq}} < -H/2$ ($z_{\mathrm{eq}} > H/2$), and the force is nonrestorative (restorative) along the radial direction. The regions in different colors are the ones in which trapping inside the bottle is possible. The parameters used in the simulation are $\lambda_0 = 780$ nm, $P = 500$ mW, $n_m = 1.46$, $n_p = 1.33$, and $p = 1$.

We can then conclude that for a given R, there is a maximum numerical aperture that can be used to form a stable trap. Conversely, for a given NA, there is a limit on the size of the particles that can be trapped. Figure 8(a) shows how this limit varies for different refractive indices of the medium and a fixed N $= 0.5$. The curves are chopped when z_{eq} becomes larger than $H/2$ and we can clearly see that the closer the refractive index gets to that of the particle, the larger is the radius of the particle that can be trapped. Figure 8 confirms that the radial force is restorative for the entire range of R and n_m that we consider. It also shows that while decreasing n_m can help to trap larger particles, it also diminishes the force experienced by the particle and hence plays an important role in the trap's stability.

D. Trapping living organisms in the dark

The bottle-beam trap finds promising applications in biology. For instance, it has been reported that organelles

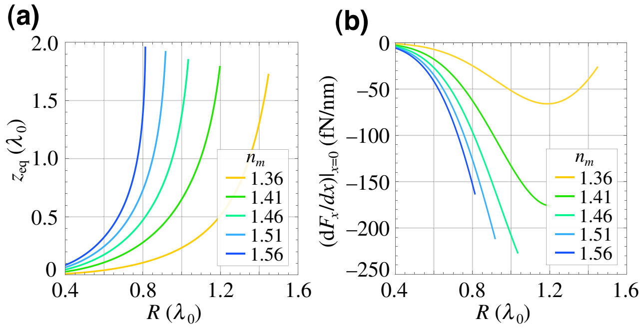

FIG. 8. Intermediate-regime simulations for different values of n_m. (a) The axial-equilibrium coordinate and (b) the first derivative of the force in the radial direction as a function of the radius of the particle. Points for which $z_{eq} > H/2$ are not displayed. The parameters used in the simulation are $\lambda_0 = 780$ nm, $P = 500$ mW, $n_m = 1.46$, $n_p = 1.33$, and $p = 1$.

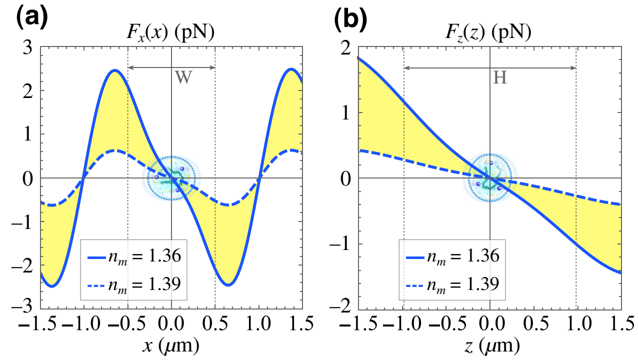

FIG. 9. The forces acting on a trapped *Mycoplasma* cell, shown here centered at the origin for size comparison, (a) along the x direction as a function of the radial displacement and (b) along the z direction as a function of the axial displacement. The solid and the dashed curves correspond to a medium's refractive index of 1.36 and 1.39, respectively, while the yellow area corresponds to $1.36 \leq n_m \leq 1.39$. The other parameters used in the simulation are displayed in Table I.

with a refractive index lower than their surroundings are repelled from standard Gaussian optical tweezers [63]. The bottle beam could then be used to manipulate such organelles within a cell.

Similarly, a dark optical trap could also be employed to trap living organisms without excessive laser damage in the cell by an appropriate choice of a surrounding medium. Iodixanol, with its high water solubility, has been reported as a nontoxic medium for different organisms, in which the refractive index can be linearly tuned in the visible to near-IR range from approximately 1.33 to approximately 1.40 by changing the concentration [64]. Assuming a mean refractive index for a living cell to be within the range from approximately 1.36 to approximately 1.39 [65,66], it is expected that stable trapping in a dark focus can be attained.

Mycoplasma are known to be among the smallest living organisms and perhaps the simplest cells [67]. With radii of around 0.3 μm, these organisms lack a cell wall [68], being protected from the surrounding environment solely by their cellular membrane. This may present interesting mechanical and elastic properties that could be probed with the bottle beam. We propose investigating the trapping of *Mycoplasma* cells immersed in a nontoxic mixture of refractive index 1.40. Iodixanol presents a possible such medium but further empirical tests must be carried out to fully determine how it affects living *Mycoplasma* cells. Figure 9 shows the simulated forces acting on a trapped *Mycoplasma* when the parameters shown in Table I are used. As can be seen, forces along radial and axial directions are restorative and should provide stable trapping inside the bottle.

It is known that direct incidence of focused laser light onto living cells can affect their division and growth [63]. As an interesting application of the bottle beam, one could observe the process of cell division without directly sending a focused beam onto the trapped particle. The following experiment could be performed: at each round of measurement, a cell undergoing division is trapped in the dark focus by a given laser power and the complete cycle of the division process is observed. A trapped dividing cell will occupy an increasing volume and unavoidably encounter the boundary of the dark region, where the trapping beam will impose a pressure against the volume expansion. By increasing the laser power used in each round, one can look for the threshold power for which cell division is precluded. With the proper tweezer calibration presented in the previous section, the threshold power provides information on the forces acting during the process of cell division.

As for the trapping beam, we note that the desired superposition can be created using a SLM, a versatile tool for shaping arbitrary amplitude and phase distributions without the need for combining aligned multiple beams. For the purpose of the present work, controlled preparation of a desired superposition of Laguerre-Gaussian modes can be

TABLE I. Proposed values for trapping a *Mycoplasma* cell using a bottle beam.

Parameter	Units	Value
Particle refractive index, n_p	···	1.36–1.39
Medium refractive index, n_m	···	1.40
Particle radius, R	μm	0.3
Laser wavelength, λ_0	nm	1064
Numerical aperture, NA	···	0.7
Laser power	mW	500
Index, p	···	1

efficiently implemented, as recently demonstrated in Ref. [35]. For the moderate NA of 0.7—much smaller than the usual value of 1.3 used when trapping particles in liquid media—we do not expect aberrations to pose a serious challenge for optical trapping with the bottle beam.

IV. CONCLUSIONS

We theoretically analyze the optical forces acting on a particle of lower refractive index than its surrounding medium trapped in the dark focus of a bottle beam generated by the superposition of a Gaussian beam and a Laguerre-Gauss beam with $\ell = 0$ and $p \neq 0$. Because the size of trapped particles commonly ranges from tens of nanometers [42] to several microns [43], we analyze such forces both for particles much smaller than and with dimensions comparable to the wavelength of the trapping beam.

In the case of small particles, the dipole approximation is applied, resulting in a number of distinguishing features of the investigated trap. Scattering is found to be null at the focus of the beam, eliminating imbalance between gradient and scattering forces [51]. The optical potential, on the other hand, couples the motion along the radial and axial directions. It is shown that these can be decoupled by using a sufficiently high trapping power. The approximated decoupled potential turns out to be quartic and quadratic in the radial and axial directions, respectively. To test the validity of the approximated potential, the motion of a particle trapped by the exact potential in a viscous medium is simulated and the results are compared with those expected from the approximation as a function of the laser power. We also show that by superposing a third mode, motion along the axial and radial directions can be decoupled independently of the trap power. To guide future experimental realizations, a calibration method is proposed.

In the case of larger objects, for which the dipole approximation is not valid, the tools developed in Refs. [44,61] are used to calculate the optical forces. Equilibrium positions after the focus are found, indicating a trapping regime different from that described in Ref. [62]. The interplay between the numerical aperture and the radius of the sphere is explored and leads to the conclusion that there is an upper bound for both of these quantities when using bottle beams for optical trapping. These limitations are interpreted in terms of the size of the optical bottle in comparison to the size of the particle and are found to be eased by choosing a medium with a refractive index close to that of the particle.

Finally, the findings obtained through exploration of the intermediate regime lead to an experimental proposal to trap a living organism using the bottle beam. Considering refractive-index values reported in the literature, it is expected that trapping of small cells such as *Mycoplasma* immersed in a nontoxic high-refractive-index medium in a dark focus is within reach. This could be applied to situations in which focusing a high laser power onto the scrutinized cell is detrimental [47], as in the case of cellular division [63].

As a final remark, we note that the present analysis could be applied to other types of bottle beams and structured beams in general. This would be specially interesting for applications dealing with micron-sized objects, since many works deal only with the case of Rayleigh particles [21–23,25,26]. Additionally, it would be interesting to explore how the dark focus affects the transfer of angular momentum between the trapping beam and the trapped particle when a superposition of circularly polarized beams or beams possessing angular momentum is used.

ACKNOWLEDGMENTS

We would like to thank Lucianno Defaveri for fruitful discussions regarding the statistical-mechanics aspects of this work. In 2019, T.G. attended the Prospects in Theoretical Physics program at the Institute for Advanced Studies in Princeton. The meeting was centered on “Great Problems in Biology for Physicists” and had an important impact on the development of this work. This study was financed in part by the Coordenação de Aperfeiçoamento de Pessoal de Nível Superior—Brasil (CAPES)—Finance Code 001, the Conselho Nacional de Desenvolvimento Científico e Tecnológico (CNPq), the Fundação de Amparo à Pesquisa do Estado do Rio de Janeiro (Faperj, Scholarships No. E-26/200.270/2020 and No. E-26/202.830/2019), the Instituto Serrapilheira (Serra-1709-21072), and the Instituto Nacional de Ciência e Tecnologia de Informação Quântica (INCT-CNPq).

APPENDIX A: TOTAL POWER OF A BOTTLE BEAM

Throughout Sec. II, we use the power P_0 of each beam in the superposition as a measure of the trapping power. To find the exact relation between P_0 and the total power of the beam, we need to integrate Eq. (7) along some plane orthogonal to the propagation of the beam. Choosing the plane $z = 0$,

$$\begin{aligned} P &= \int_0^\infty d\rho \int_0^{2\pi} (d\theta\rho) I_0 e^{-2\rho^2/\omega_0^2} \\ &\quad \times \left[1 - 2L_p^0\left(\frac{2\rho^2}{\omega_0^2}\right) + L_p^0\left(\frac{2\rho^2}{\omega_0^2}\right)^2\right] \\ &= 2\pi I_0 \int_0^\infty \frac{\omega_0^2 du}{4} e^{-u}[1 - 2L_p^0(u) + L_p^0(u)^2] \\ &= P_0 \int_0^\infty du\, e^{-u}[1 - 2L_p^0(u) + L_p^0(u)^2]. \qquad \text{(A1)} \end{aligned}$$

The Laguerre-Polynomials satisfy

$$\int_0^\infty x^\ell e^{-x} L_p^{|\ell|}(x) L_q^{|\ell|}(x) = \frac{(p+\ell)!}{p!}\delta_{p,q}, \tag{A2}$$

which implies that

$$\int_0^\infty du\, e^{-u} = \int_0^\infty du\, e^{-u} L_0^0(u) L_0^0(u) = 1, \tag{A3}$$

$$\int_0^\infty du\, e^{-u} L_p^0(u) = \int_0^\infty du\, e^{-u} L_0^0(u) L_p^0(u) = 0, \tag{A4}$$

$$\int_0^\infty du\, e^{-u} L_p^0(u)^2 = \int_0^\infty du\, e^{-u} L_p^0(u) L_p^0(u) = 1. \tag{A5}$$

Finally, substituting Eqs. (A3)–(A5) into Eq. (A1), we find that

$$P = 2P_0. \tag{A6}$$

APPENDIX B: THE DECOUPLING MODE

In this appendix, we derive the conditions that must be fulfilled by a three-mode superposition in order to provide a decoupled potential for the trapped particles, while keeping the bottle-beam structure. Let us consider the superposition

$$E(\rho,z) = E_{0,0}^{\mathrm{LG}}(\rho,z) + \alpha_1 E_{0,p_1}^{\mathrm{LG}}(\rho,z) + \alpha_2 E_{0,p_2}^{\mathrm{LG}}(\rho,z). \tag{B1}$$

We want to obtain a relationship between the complex coefficients α_1 and α_2 and the radial orders p_1 and p_2 that achieves the desired decoupling and bottle-beam profile. The LG modes with zero orbital angular momentum are given by

$$E_{0,p}^{\mathrm{LG}}(\bar\rho,\bar z) = \frac{\mathcal{N}}{\sqrt{1+\bar z^2}} e^{-\frac{\bar\rho^2}{2}} L_p^0\left(\bar\rho^2\right)\left(\frac{1-i\bar z}{\sqrt{1+\bar z^2}}\right)^{2p+1} \times \exp\left[ikz + ik\frac{\rho^2}{2R(z)}\right], \tag{B2}$$

where we define $\mathcal{N} = \sqrt{4P_0/c\epsilon\pi\omega_0^2}$, $\bar\rho = \sqrt{2}\rho/w(z)$, and $\bar z = z/z_R$ and the last term is the Gouy phase.

The trapping potential is proportional to the light-intensity distribution and, therefore, to the square modulus of the electric field:

$$I(\bar\rho,\bar z) = \frac{I_0}{1+\bar z^2} e^{-\bar\rho^2}\left|1 + \alpha_1 L_{p_1}^0\left(\bar\rho^2\right)\left(\frac{1-i\bar z}{\sqrt{1+\bar z^2}}\right)^{2p_1} + \alpha_2 L_{p_2}^0\left(\bar\rho^2\right)\left(\frac{1-i\bar z}{\sqrt{1+\bar z^2}}\right)^{2p_2}\right|^2. \tag{B3}$$

We seek an approximate expression for the trapping potential around the beam focus, which can be obtained from a power-series expansion around this point. The bottle-beam condition requires that the light intensity vanishes at the focus. Note that $L_p^0(0) = 1$, so the light intensity at the beam focus is proportional to

$$I(\mathbf{0}) = I_0\left|1+\alpha_1+\alpha_2\right|^2, \tag{B4}$$

which implies that

$$\left|1+\alpha_1+\alpha_2\right|^2 = 0. \tag{B5}$$

This condition cancels out the zero-order contribution to the power-series expansion. We keep terms up to $\bar\rho^4$ and $\bar z^2$, which are the first nonvanishing contributions to the power series. Since the zero-order term vanishes, it will be easier to first expand the expression inside the square modulus in Eq. (B3) and keep terms up to $\bar\rho^2$ and $\bar z^2$. The following approximations are assumed:

$$e^{-\bar\rho^2} \approx 1 - \bar\rho^2, \tag{B6}$$

$$L_p^0\left(\bar\rho^2\right) \approx 1 - p\bar\rho^2, \tag{B7}$$

$$\left(\frac{1-i\bar z}{\sqrt{1+\bar z^2}}\right)^{2p} \approx 1 - 2ip\bar z - 2p^2\bar z^2, \tag{B8}$$

$$\frac{1}{1+\bar z^2} \approx 1 - \bar z^2. \tag{B9}$$

Applying the approximations above together with the bottle-beam condition (B5), we find the following approximate expression for the trapping intensity:

$$\begin{aligned}
I(\bar\rho,\bar z) &\approx I_0\left(1-\bar\rho^2\right)\left|2A\bar z(\bar z - i\bar\rho^2) + B(\bar\rho^2 + 2i\bar z)\right|^2 \\
&\approx I_0\left[|B|^2(4\bar z^2 + \bar\rho^4) - 4\{|B|^2 + \mathrm{Re}\left(AB^*\right)\}\bar\rho^2\bar z^2\right] \\
&\approx I_0\left[4|B|^2\left(\frac{z^2}{z_R^2} + \frac{\rho^4}{w_0^4}\right) - 8\left[|B|^2 + \mathrm{Re}\left(AB^*\right)\right]\frac{z^2\rho^2}{z_R^2 w_0^2}\right],
\end{aligned}$$

where we define

$$A = \alpha_1 p_1^2 + \alpha_2 p_2^2, \tag{B10}$$

$$B = \alpha_1 p_1 + \alpha_2 p_2. \tag{B11}$$

The two-mode bottle-beam potential is recovered by making $\alpha_1 = -1$ and $\alpha_2 = 0$.

Decoupling between the radial (ρ) and longitudinal (z) dependencies is achieved by choosing α_1 and α_2 such that

$$|B|^2 + \mathrm{Re}\left(AB^*\right) = 0 \quad (B \neq 0). \tag{B12}$$

We can write this condition in terms of the real and imaginary parts of the coefficients $\alpha_j = a_j + ib_j$. Including the bottle-beam condition, the following equations must hold:

$$1 + a_1 + a_2 = 0, \tag{B13}$$

$$b_1 + b_2 = 0, \tag{B14}$$

$$(a_1^2 + b_1^2)(p_1^2 + p_1^3) + (a_2^2 + b_2^2)(p_2^2 + p_2^3) + p_1p_2(p_1 + p_2 + 2)(a_1a_2 + b_1b_2) = 0. \tag{B15}$$

By using (B13) and (B14) in (B15), we derive the following condition:

$$(a_1^2 + b_1^2)\left[p_1^2(p_1 + 1) + p_2^2(p_2 + 1) - p_1p_2(p_1 + p_2 + 2)\right] + a_1\left[2p_2^2(p_2 + 1) - p_1p_2(p_1 + p_2 + 2)\right] + p_2^2(p_2 + 1) = 0. \tag{B16}$$

For example, let us set $p_1 = 1$ and $p_2 = 2$, giving

$$a_1^2 + b_1^2 + \frac{7}{2}a_1 + 3 = 0 \Rightarrow b_1^2 = -\left(a_1^2 + \frac{7}{2}a_1 + 3\right) \geq 0. \tag{B17}$$

This condition has infinite solutions in the interval $-2 \leq a_1 \leq -3/2$. Its limits provide real solutions for the superposition coefficients:

(a) $\alpha_1 = -2$, $\alpha_2 = 1$.
(b) $\alpha_1 = -3/2$, $\alpha_2 = 1/2$.

Note that the first real solution is useless, since it gives $B = 0$ and cancels out all terms up to ρ^4 and z^2 in the trapping potential. The other real solution gives $A = 1/2$ and $B = -1/2$, resulting in the following expression for intensity of the electric field:

$$I(\rho, z) \approx I_0\left(\frac{z^2}{z_R^2} + \frac{\rho^4}{w_0^4}\right), \tag{B18}$$

which provides the desired bottle-beam configuration with decoupled dynamics along the transverse and longitudinal directions. Moreover, we can easily show that this solution is optimal. Under the bottle-beam and decoupling condition, the trapping strength is

$$4|B|^2 = 2a_1 + 4, \tag{B19}$$

which is a linear function of a_1 with positive slope. Therefore, its maximum value is obtained at the upper limit $a_1 = -3/2$.

[1] A. Ashkin, J. M. Dziedzic, J. E. Bjorkholm, and S. Chu, Observation of a single-beam gradient force optical trap for dielectric particles, Opt. Lett. **11**, 288 (1986).

[2] F. M. Fazal and S. M. Block, Optical tweezers study life under tension, Nat. Photonics **5**, 318 (2011).

[3] H. M. Nussenzveig, Cell membrane biophysics with optical tweezers, Eur. Biophys. J. **47**, 499 (2017).

[4] G. R. de S. Araújo, N. B. Viana, F. Gómez, B. Pontes, and S. Frases, The mechanical properties of microbial surfaces and biofilms, Cell Surface **5**, 100028 (2019).

[5] B. Pontes, Y. Ayala, A. C. C. Fonseca, L. F. Romão, R. F. Amaral, L. T. Salgado, F. R. Lima, M. Farina, N. B. Viana, V. Moura-Neto, and H. M. Nussenzveig, Membrane elastic properties and cell function, PLoS ONE **8**, e67708 (2013).

[6] F. Monteiro, W. Li, G. Afek, C.-L. Li, M. Mossman, and D. C. Moore, Force and acceleration sensing with optically levitated nanogram masses at microkelvin temperatures, Phys. Rev. A **101**, 053835 (2020).

[7] D. S. Ether, L. B. Pires, S. Umrath, D. Martinez, Y. Ayala, B. Pontes, G. R. de S. Araújo, S. Frases, G.-L. Ingold, F. S. S. Rosa, N. B. Viana, H. M. Nussenzveig, and P. A. M. Neto, Probing the Casimir force with optical tweezers, EPL **112**, 44001 (2015).

[8] A. Arvanitaki and A. A. Geraci, Detecting High-Frequency Gravitational Waves with Optically Levitated Sensors, Phys. Rev. Lett. **110**, 071105 (2013).

[9] A. A. Geraci, S. B. Papp, and J. Kitching, Short-Range Force Detection Using Optically Cooled Levitated Microspheres, Phys. Rev. Lett. **105**, 101101 (2010).

[10] D. C. Moore, A. D. Rider, and G. Gratta, Search for Millicharged Particles Using Optically Levitated Microspheres, Phys. Rev. Lett. **113**, 251801 (2014).

[11] A. Ashkin, Acceleration and Trapping of Particles by Radiation Pressure, Phys. Rev. Lett. **24**, 156 (1970).

[12] B. P. S. Ahluwalia, X.-C. Yuan, S. H. Tao, W. C. Cheong, L. S. Zhang, and H. Wang, Micromanipulation of high and low indices microparticles using a microfabricated double axicon, J. Appl. Phys. **99**, 113104 (2006).

[13] G. Li, S. Zhang, L. Isenhower, K. Maller, and M. Saffman, Crossed vortex bottle beam trap for single-atom qubits, Opt. Lett. **37**, 851 (2012).

[14] O. Aldossary, Bottle atom trapping configuration by optical dipole forces, J. King Saud Univ. Sci. **26**, 29 (2014).

[15] D. Barredo, V. Lienhard, P. Scholl, S. de Léséleuc, T. Boulier, A. Browaeys, and T. Lahaye, Three-Dimensional Trapping of Individual Rydberg Atoms in Ponderomotive Bottle Beam Traps, Phys. Rev. Lett. **124**, 023201 (2020).

[16] P. Xu, X. He, J. Wang, and M. Zhan, Trapping a single atom in a blue detuned optical bottle beam trap, Opt. Lett. **35**, 2164 (2010).

[17] J. Arlt and M. J. Padgett, Generation of a beam with a dark focus surrounded by regions of higher intensity: The optical bottle beam, Opt. Lett. **25**, 191 (2000).

[18] J. Arlt, K. Dholakia, J. Soneson, and E. M. Wright, Optical dipole traps and atomic waveguides based on Bessel light beams, Phys. Rev. A **63**, 063602 (2001).

[19] R. A. B. Suarez, L. A. Ambrosio, A. A. R. Neves, M. Zamboni-Rached, and M. R. R. Gesualdi, Experimental optical trapping with frozen waves, Opt. Lett. **45**, 2514 (2020).

[20] W. Lu, X. Sun, H. Chen, S. Liu, and Z. Lin, Abruptly autofocusing property and optical manipulation of circular Airy beams, Phys. Rev. A **99**, 013817 (2019).

[21] H. Cheng, W. Zang, W. Zhou, and J. Tian, Analysis of optical trapping and propulsion of Rayleigh particles using Airy beam, Opt. Express **18**, 20384 (2010).

[22] Y. Jiang, K. Huang, and X. Lu, Radiation force of abruptly autofocusing Airy beams on a Rayleigh particle, Opt. Express **21**, 24413 (2013).

[23] J. Shu, Z. Chen, and J. Pu, Radiation forces on a Rayleigh particle by highly focused partially coherent and radially polarized vortex beams, J. Opt. Soc. Am. A **30**, 916 (2013).

[24] S. Yan and B. Yao, Radiation forces of a highly focused radially polarized beam on spherical particles, Phys. Rev. A **76**, 053836 (2007).

[25] C. Zhao, Y. Cai, X. Lu, and H. T. Eyyuboğlu, Radiation force of coherent and partially coherent flat-topped beams on a Rayleigh particle, Opt. Express **17**, 1753 (2009).

[26] D. Zhang and Y. Yang, Radiation forces on Rayleigh particles using a focused anomalous vortex beam under paraxial approximation, Opt. Commun. **336**, 202 (2015).

[27] C.-L. Zhao, L.-G. Wang, and X.-H. Lu, Radiation forces on a dielectric sphere produced by highly focused hollow Gaussian beams, Phys. Lett. A **363**, 502 (2007).

[28] C. Zhao, Y. Cai, and O. Korotkova, Radiation force of scalar and electromagnetic twisted Gaussian Schell-model beams, Opt. Express **17**, 21472 (2009).

[29] C. Zhao and Y. Cai, Trapping two types of particles using a focused partially coherent elegant Laguerre-Gaussian beam, Opt. Lett. **36**, 2251 (2011).

[30] Q. Zhan, Radiation forces on a dielectric sphere produced by highly focused cylindrical vector beams, J. Opt. A: Pure Appl. Opt. **5**, 229 (2003).

[31] M.-D. Wei, W.-L. Shiao, and Y.-T. Lin, Adjustable generation of bottle and hollow beams using an axicon, Opt. Commun. **248**, 7 (2005).

[32] J.-H. Lin, M.-D. Wei, H.-H. Liang, K.-H. Lin, and W.-F. Hsieh, Generation of supercontinuum bottle beam using an axicon, Opt. Express **15**, 2940 (2007).

[33] T. Du, T. Wang, and F. Wu, Generation of three-dimensional optical bottle beams via focused non-diffracting Bessel beam using an axicon, Opt. Commun. **317**, 24 (2014).

[34] L. Isenhower, W. Williams, A. Dally, and M. Saffman, Atom trapping in an interferometrically generated bottle beam trap, Opt. Lett. **34**, 1159 (2009).

[35] B. P. da Silva, V. A. Pinillos, D. S. Tasca, L. E. Oxman, and A. Z. Khoury, Pattern Revivals from Fractional Gouy Phases in Structured Light, Phys. Rev. Lett. **124**, 033902 (2020).

[36] B. Ahluwalia, X.-C. Yuan, and S. Tao, Generation of self-imaged optical bottle beams, Opt. Commun. **238**, 177 (2004).

[37] P. Zhang, Z. Zhang, J. Prakash, S. Huang, D. Hernandez, M. Salazar, D. N. Christodoulides, and Z. Chen, Trapping and transporting aerosols with a single optical bottle beam generated by Moiré techniques, Opt. Lett. **36**, 1491 (2011).

[38] N. Matsumoto, T. Ando, T. Inoue, Y. Ohtake, N. Fukuchi, and T. Hara, Generation of high-quality higher-order Laguerre-Gaussian beams using liquid-crystal-on-silicon spatial light modulators, J. Opt. Soc. Am. A **25**, 1642 (2008).

[39] Y. Ohtake, T. Ando, N. Fukuchi, N. Matsumoto, H. Ito, and T. Hara, Universal generation of higher-order multiringed Laguerre-Gaussian beams by using a spatial light modulator, Opt. Lett. **32**, 1411 (2007).

[40] D. P. Rhodes, D. M. Gherardi, J. Livesey, D. McGloin, H. Melville, T. Freegarde, and K. Dholakia, Atom guiding along high order Laguerre-Gaussian light beams formed by spatial light modulation, J. Mod. Opt. **53**, 547 (2006).

[41] T. Ando, Y. Ohtake, N. Matsumoto, T. Inoue, and N. Fukuchi, Mode purities of Laguerre-Gaussian beams generated via complex-amplitude modulation using phase-only spatial light modulators, Opt. Lett. **34**, 34 (2008).

[42] P. M. Hansen, V. K. Bhatia, N. Harrit, and L. Oddershede, Expanding the optical trapping range of gold nanoparticles, Nano Lett. **5**, 1937 (2005).

[43] H. G. Alinezhad and S. N. S. Reihani, Optimal condition for optical trapping of large particles: Tuning the laser power and numerical aperture of the objective, J. Opt. Soc. Am. B **36**, 3053 (2019).

[44] T. A. Nieminen, V. L. Y. Loke, A. B. Stilgoe, G. Knöner, A. M. Brańczyk, N. R. Heckenberg, and H. Rubinsztein-Dunlop, Optical tweezers computational toolbox, J. Opt. A: Pure Appl. Opt. **9**, S196 (2007).

[45] Y. Liu, D. Cheng, G. Sonek, M. Berns, C. Chapman, and B. Tromberg, Evidence for localized cell heating induced by infrared optical tweezers, Biophys. J. **68**, 2137 (1995).

[46] E. J. Peterman, F. Gittes, and C. F. Schmidt, Laser-induced heating in optical traps, Biophys. J. **84**, 1308 (2003).

[47] A. Blázquez-Castro, Optical tweezers: Phototoxicity and thermal stress in cells and biomolecules, Micromachines **10**, 507 (2019).

[48] T. Li, *Fundamental Tests of Physics with Optically Trapped Microspheres* (Springer, New York, 2013).

[49] P. H. Jones, O. M. Marago, and G. Volpe, *Optical Tweezers* (Cambridge University Press, Cambridge, 2015).

[50] S. Albaladejo, M. I. Marqués, M. Laroche, and J. J. Sáenz, Scattering Forces from the Curl of the Spin Angular Momentum of a Light Field, Phys. Rev. Lett. **102**, 113602 (2009).

[51] T. A. Nieminen, N. R. Heckenberg, and H. Rubinsztein-Dunlop, Forces in optical tweezers with radially and azimuthally polarized trapping beams, Opt. Lett. **33**, 122 (2008).

[52] G. M. Gibson, J. Leach, S. Keen, A. J. Wright, and M. J. Padgett, Measuring the accuracy of particle position and force in optical tweezers using high-speed video microscopy, Opt. Express **16**, 14561 (2008).

[53] A. Pralle, M. Prummer, E.-L. Florin, E. Stelzer, and J. Hörber, Three-dimensional high-resolution particle tracking for optical tweezers by forward scattered light, Microsc. Res. Tech. **44**, 378 (1999).

[54] P. S. Alves and M. S. Rocha, Videomicroscopy calibration of optical tweezers by position autocorrelation function analysis, Appl. Phys. B **107**, 375 (2012).

[55] K. Berg-Sørensen and H. Flyvbjerg, Power spectrum analysis for optical tweezers, Rev. Sci. Instrum. **75**, 594 (2004).

[56] B. Melo, F. Almeida, G. Temporão, and T. Guerreiro, Relaxing constraints on data acquisition and position detection for trap stiffness calibration in optical tweezers, Opt. Express **28**, 16256 (2020).

[57] R. Simmons, J. Finer, S. Chu, and J. Spudich, Quantitative measurements of force and displacement using an optical trap, Biophys. J. **70**, 1813 (1996).

[58] G. Brouhard, H. Schek, and A. Hunt, Advanced optical tweezers for the study of cellular and molecular biomechanics, IEEE. Trans. Biomed. Eng. **50**, 121 (2003).

[59] M.-C. Zhong, X.-B. Wei, J.-H. Zhou, Z.-Q. Wang, and Y.-M. Li, Trapping red blood cells in living animals using optical tweezers, Nat. Commun. **4**, 1768 (2013).

[60] Y. Liang, G. Liang, Y. Xiang, J. Lamstein, R. Gautam, A. Bezryadina, and Z. Chen, Manipulation and Assessment of Human Red Blood Cells with Tunable "Tug-of-War" Optical Tweezers, Phys. Rev. Appl. **12**, 064060 (2019).

[61] I. C. D. Lenton, T. A. Nieminen, V. L. Y. Loke, A. B. Stilgoe, Y. Hu, G. Knöner, A. M. Brańczyk, N. R. Heckenberg, and H. Rubinsztein-Dunlop, Optical tweezers toolbox (2020).

[62] K. T. Gahagan and G. A. Swartzlander, Optical vortex trapping of particles, Opt. Lett. **21**, 827 (1996).

[63] H. Zhang and K.-K. Liu, Optical tweezers for single cells, J. R. Soc. Interface **5**, 671 (2008).

[64] T. Boothe, L. Hilbert, M. Heide, L. Berninger, W. B. Huttner, V. Zaburdaev, N. L. Vastenhouw, E. W. Myers, D. N. Drechsel, and J. C. Rink, A tunable refractive index matching medium for live imaging cells, tissues and model organisms, eLife **6**, e27240 (2017).

[65] P. Y. Liu, L. K. Chin, W. Ser, H. F. Chen, C.-M. Hsieh, C.-H. Lee, K.-B. Sung, T. C. Ayi, P. H. Yap, B. Liedberg, K. Wang, T. Bourouina, and Y. Leprince-Wang, Cell refractive index for cell biology and disease diagnosis: Past, present and future, Lab. Chip **16**, 634 (2016).

[66] B. Rappaz, P. Marquet, E. Cuche, Y. Emery, Depeursinge, and P. J. Magistretti, Measurement of the integral refractive index and dynamic cell morphometry of living cells with digital holographic microscopy, Opt. Express **13**, 9361 (2005).

[67] H. J. Morowitz, The completeness of molecular biology, Isr. J. Med. Sci. **20**, 750 (1984).

[68] D. C. Krause and M. F. Balish, Structure, function, and assembly of the terminal organelle of *Mycoplasma pneumoniae*, FEMS Microbiol. Lett. **198**, 1 (2001).